arXiv:1609.08499v1 [cond-mat.quant-gas] 27 Sep 2016

Magnetic solitons in Rabi-coupled Bose-Einstein condensates

Chunlei Qu[1],* Marek Tylutki[1], Sandro Stringari[1], and Lev P. Pitaevskii[1,2]
[1] *INO-CNR BEC Center and Dipartimento di Fisica, Università di Trento, 38123 Povo, Italy*
[2] *Kapitza Institute for Physical Problems RAS, Kosygina 2, 119334 Moscow, Russia*
(Dated: September 28, 2016)

We study magnetic solitons, solitary waves of spin polarization (i.e, magnetization), in binary Bose-Einstein condensates in the presence of Rabi coupling. We show that the system exhibits two types of magnetic solitons, called 2π and 0π solitons, characterized by a different behavior of the relative phase between the two spin components. 2π solitons exhibit a 2π jump of the relative phase, independent of their velocity, the static domain wall explored by Son and Stephanov being an example of such 2π solitons with vanishing velocity and magnetization. 0π solitons do not instead exhibit any asymptotic jump in the relative phase. Systematic results are provided for both types of solitons in uniform matter. Numerical calculations in the presence of a one dimensional harmonic trap reveal that a 2π soliton evolves in time into a 0π soliton, and vice versa, oscillating around the center of the trap. Results for the effective mass, the Landau critical velocity and the role of the transverse confinement are also discussed.

I. INTRODUCTION

Topological defects are nontrivial collective excitations that appear in a wide variety of systems in different physical branches including classical fluids, cosmology [1], condensed matter [2, 3], optics [4], cold atoms [5], etc. Despite the fact that they do not correspond to the ground states of the systems, these topological defects can be stable and live for a long time under certain physical conditions, which may have important applications for information processing. Because of the tunability of the interaction coupling constants and the absence of disorder, ultracold atomic gases provide an ideal playground for the observation of these excitations. Since the first realization of Bose-Einstein condensate with alkali atoms, various topological defects have been experimentally observed and/or theoretically investigated, such as scalar solitons [6–8], vector solitons [9–12], domain walls [13], vortices [14, 15], skyrmions [16, 17], etc.

The application of a coherent coupling between two internal states is a powerful tool for the control of spinor condensates with external fields [18, 19]. In this work, we shall consider a Rabi-coupled two-component Bose-Einstein condensate, the corresponding topological defects being intrinsically different from those in the absence of Rabi coupling [20, 21]. Useful simplifications in the determination of the solitonic solutions in uniform matter take place when the intra-species coupling constants are equal ($g \equiv g_{11} = g_{22}$) and very close to the inter-species coupling g_{12}, i.e.

$$\delta g \equiv g - g_{12} \ll g \tag{1}$$

with $\delta g > 0$ in order to ensure miscibility even in the absence of Rabi coupling [22]. The condition (1) ensures that the total density $n = n_1 + n_2$ is not affected by the presence of the soliton, thereby reducing the relevant variables of the problem to the spin density $n_1 - n_2$ and to the phases of the two spin components. For this reason the corresponding solutions will be called magnetic solitons. The condition (1) is fulfilled, for example, by the $|F = 1; m_F = \pm 1\rangle$ hyperfine states of ^{23}Na.

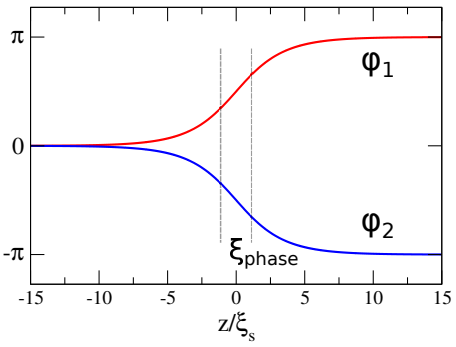

FIG. 1. Phase structure of the static Son-Stephanov domain wall. The relative phase of the two spin states exhibits a 2π jump when one moves from $-\infty$ to $+\infty$. The width of the domain wall is fixed by the characteristic length of the relative phase $\xi_{\rm phase} = \sqrt{\hbar/2m\Omega}$, where Ω is the Rabi coupling.

We notice that magnetic solitons have been already predicted in the absence of Rabi-coupling where the relative phase of the two components exhibits a π phase jump across the soliton [23] (see also Ref. [24] for more general solutions available under the same condition (1)). In the presence of Rabi coupling, the relative phase φ_A should satisfy the condition $\cos\varphi_A = 1$ at large distances from the soliton, which implies that the jump of the relative phase must be equal to $2n\pi$ with $n = 0, 1, \ldots$

A prominent example of solitonic solution in a Rabi-coupled binary condensate is the static domain wall identified by Son and Stephanov in 2002 [13] by considering two equally populated spin states coupled by a weak Rabi-coupling of strength Ω in uniform matter. Under the assumption (1) these authors found a metastable solution, corresponding to a local minimum of the en-

* chunleiqu@gmail.com

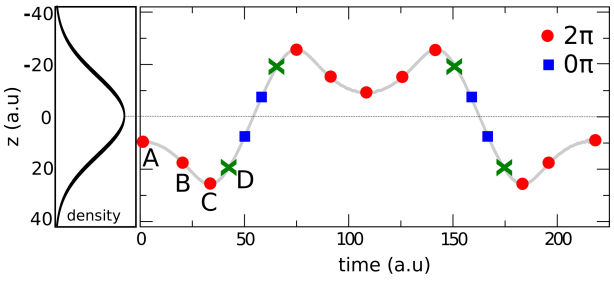

FIG. 2. Illustration of the dynamics of magnetic solitons in a harmonic trap. At $t = 0$, a static Son-Stephanov domain wall, characterized by a 2π jump in the relative phase, is imprinted on the right (point A) of the trap center . The 2π soliton starts moving towards the periphery and, soon after the reflection, it evolves into a 0π soliton (point D) (see text). 2π solitons are indicated with red circles, while 0π solitons are indicated with blue squares. The green crosses are points indicating the transformation between 2π and 0π solitons.

ergy functional, characterized by the 2π jump of the relative phase of the two components across the wall (see Fig. 1). This static soliton is characterized by the absence of magnetization and corresponds to a metastable solution of the coupled Gross-Pitaevskii equations (GPEs) if the condition

$$\hbar\Omega < \hbar\Omega_c \equiv \frac{1}{3} n\delta g, \tag{2}$$

is satisfied. For larger values of Ω the static domain wall corresponds to a local maximum of the energy functional and the resulting configuration is consequently unstable in uniform matter [13].

The absence of magnetization of the static domain wall makes its experimental detection difficult. In this work we will show that the Son-Stephanov domain wall exhibits a magnetization when it moves, thereby opening realistic perspectives for its experimental detection.

In order to generate moving magnetic solitons we found it convenient to imprint the phase of the static Son-Stephanov domain wall (see Fig. 1), with its center displaced from the center of the trap (see Fig. 2) and to follow the numerical evolution of the time dependent GPEs. Initially the densities of the two components of the mixture have the same profile, yielding a vanishing value of magnetization. Once the domain wall moves, a non-vanishing magnetization is formed giving rise to a soliton which also exhibits a 2π jump in the relative phase (2π soliton). Thus the velocity plays the role of an effective magnetic field, polarizing the soliton. As time evolves the position of the soliton moves towards the periphery of the trapped gas and increases its velocity as a consequence of the fact that its effective mass is positive. Before reaching the border of the condensate the soliton however slowers as a consequence of the fact that its effective mass at some intermediate point, indicated with the letter B in Fig. 2, changes sign and becomes negative. Eventually the soliton reaches a zero velocity (indicated with the letter C in Fig. 2) and is thereafter reflected towards the center of the trap. When the Rabi-coupling is much smaller than the critical value in Eq. (2), soon after the inversion of the velocity, the 2π soliton exhibits a deep transformation characterized by a drastic change of its phase and is transformed into a 0π soliton which does not exhibit an asymptotic phase jump in the relative phase. This transformation takes place when the local magnetization at the center of the soliton is equal to 1, which means that the density of one of the spin components exactly vanishes (the cross point indicated with the letter D in Fig. 2). The 0π soliton is then accelerated toward the center of the trap and decelerated when it starts reaching the region of lower density, on the opposite side of the trap, as a consequence of the negativity of its effective mass. The 0π soliton cannot reach zero velocity and at some point is transformed again into a 2π soliton which eventually reaches zero velocity to be reflected again. This highly non trivial dynamical behavior is illustrated in Fig. 2 where the position of the soliton is shown as a function of time.

The above concise description of the dynamics of magnetic solitons permits to understand the structure of the paper which is organized as follows:

In Sec. II, we formulate a variational approach to the time dependent GPEs, allowing for the identification of the solitonic solutions. In Sec. III, we derive analytic results for the static and moving Son-Stephanov domain wall (2π soliton) in the presence of weak Rabi coupling. The general solutions of the 2π and 0π moving magnetic solitons are discussed in Sec. IV. The phase diagram and the properties of the magnetic solitons are discussed in Sec. V. Then we discuss the dynamics and stability of the solitons in a one-dimensional (1D) harmonic trap (Sec. VI) as well as in the presence of an additional transverse confinement (Sec. VII). Sec. VIII is devoted to the final discussions and conclusions.

II. SOLITONS IN UNIFORM MATTER

A. Equations for the magnetic solitons

A two-component Bose-Einstein condensate in the presence of Rabi-coupling is governed by two coupled GPEs which can be derived from the following Lagrangian density

$$\mathcal{L} = \sum_{j=1}^{2} \frac{i\hbar}{2}\left(\psi_j^* \frac{\partial}{\partial t}\psi_j - \psi_j \frac{\partial}{\partial t}\psi_j^*\right) - \mathcal{H}, \tag{3}$$

where $\psi_{j=1,2}$ are the wave functions of the two components and $\mathcal{H}$ is the Hamiltonian density given by

$$\mathcal{H} = \frac{\hbar^2}{2m}|\nabla\psi_1|^2 + \frac{\hbar^2}{2m}|\nabla\psi_2|^2 - \frac{1}{2}\hbar\Omega(\psi_1^*\psi_2 + \psi_2^*\psi_1) + \frac{g}{2}|\psi_1|^4 + \frac{g}{2}|\psi_2|^4 + g_{12}|\psi_1|^2|\psi_2|^2. \tag{4}$$

In this work, we have assumed the Rabi coupling parameter $\Omega > 0$. Under the condition of Eq. (1) the total

density $n = n_1 + n_2$ of the condensate exhibiting the magnetic solitonic features can be assumed to be constant [23]. As a consequence we can make the following ansatz for the spinor order parameter

$$\begin{pmatrix} \psi_1 \\ \psi_2 \end{pmatrix} = \sqrt{n} \begin{pmatrix} \cos(\theta/2) e^{i\varphi_1} \\ \sin(\theta/2) e^{i\varphi_2} \end{pmatrix}, \tag{5}$$

where $\varphi_{j=1,2}$ are the phases of the two wave functions. The densities of the two components are given by $n_{1,2} = n(1 \pm \cos\theta)/2$, and the magnetization m is calculated as $m = (n_1 - n_2)/n = \cos\theta$. Substituting Eq. (5) into the Lagrangian density Eq. (3), we obtain [13]

$$\begin{aligned} \mathcal{L} = &-n\hbar \left[\cos^2 \frac{\theta}{2} \frac{\partial \varphi_1}{\partial t} + \sin^2 \frac{\theta}{2} \frac{\partial \varphi_2}{\partial t} \right] - \frac{n\hbar^2}{2m} \left[\frac{1}{4} (\nabla\theta)^2 \right. \\ &\left. + \cos^2 \frac{\theta}{2} (\nabla\varphi_1)^2 + \sin^2 \frac{\theta}{2} (\nabla\varphi_2)^2 \right] - \frac{1}{2} n^2 g \\ &+ \frac{1}{4} n^2 \delta g \sin^2\theta + \frac{1}{2} n\hbar\Omega \sin\theta \cos(\varphi_1 - \varphi_2). \end{aligned} \tag{6}$$

It is convenient to introduce the relative and total phases of the two components

$$\varphi_A = \varphi_1 - \varphi_2, \quad \varphi_B = \varphi_1 + \varphi_2, \tag{7}$$

in terms of which, the Lagrangian density can be rewritten as

$$\begin{aligned} \mathcal{L} = &-\frac{n\hbar}{2} \left(\cos\theta \partial_t \varphi_A + \partial_t \varphi_B \right) - \frac{n\hbar^2}{8m} \left[2\cos\theta \nabla\varphi_A \nabla\varphi_B \right. \\ &\left. + (\nabla\varphi_A)^2 + (\nabla\varphi_B)^2 + (\nabla\theta)^2 \right] - \frac{1}{2} n^2 g \\ &+ \frac{1}{4} n^2 \delta g \sin^2\theta + \frac{1}{2} n\hbar\Omega \sin\theta \cos\varphi_A. \end{aligned} \tag{8}$$

It is important to note that the term $\partial_t \varphi_B$, as a derivative, does not contribute to equations of motion and thus will be omitted in the following.

We begin our discussion by considering the 1D problem where all the quantities only depend on the spatial coordinate z. We look for travelling solutions of the form $\varphi_{A,B} = \varphi_{A,B}(z - Vt)$ and $\theta = \theta(z - Vt)$ so that the Lagrangian density can be rewritten as

$$\begin{aligned} \mathcal{L} = &\frac{n\hbar V}{2} \cos\theta \frac{\partial \varphi_A}{\partial z} - \frac{n\hbar^2}{8m} \left[2\cos\theta \frac{\partial \varphi_A}{\partial z} \frac{\partial \varphi_B}{\partial z} + \left(\frac{\partial \varphi_A}{\partial z} \right)^2 \right. \\ &\left. + \left(\frac{\partial \varphi_B}{\partial z} \right)^2 + \left(\frac{\partial \theta}{\partial z} \right)^2 \right] - \frac{1}{2} n^2 g + \frac{1}{4} n^2 \delta g \sin^2\theta \\ &+ \frac{1}{2} n\hbar\Omega \sin\theta \cos\varphi_A. \end{aligned} \tag{9}$$

It is instructive to reduce the Lagrangian density to a dimensionless form. To this purpose, due to the magnetic nature of the solitons, the natural units for the coordinates and velocities will be chosen, respectively, as the spin healing length and the spin sound velocity defined in the absence of Rabi coupling:

$$\xi_s = \frac{\hbar}{\sqrt{2mn\delta g}}, \qquad c_s = \sqrt{\frac{n\delta g}{2m}}.$$

With the help of the following dimensionless variables for the position, velocity and Rabi-coupling

$$\zeta = (z - Vt)/\xi_s, \qquad U = V/c_s, \qquad \omega_R = \frac{\Omega}{\Omega_c},$$

the dimensionless Lagrangian density $\tilde{\mathcal{L}} = \mathcal{L}/nmc_s^2$ is given by

$$\begin{aligned} \tilde{\mathcal{L}} = &U\cos\theta \frac{\partial \varphi_A}{\partial \zeta} - \frac{1}{2} \left[\left(\frac{\partial \varphi_A}{\partial \zeta} \right)^2 + \left(\frac{\partial \varphi_B}{\partial \zeta} \right)^2 \right. \\ &\left. + \left(\frac{\partial \theta}{\partial \zeta} \right)^2 + 2\cos\theta \frac{\partial \varphi_A}{\partial \zeta} \frac{\partial \varphi_B}{\partial \zeta} \right] - \frac{g}{\delta g} \\ &+ \frac{1}{2} \sin^2\theta + \frac{\omega_R}{3} \sin\theta \cos\varphi_A. \end{aligned} \tag{10}$$

Variation of the Lagrangian density with respect to the total phase φ_B gives

$$\partial_\zeta \left(\frac{\partial \tilde{\mathcal{L}}}{\partial (\partial_\zeta \varphi_B)} \right) = \partial_\zeta (\partial_\zeta \varphi_B + \cos\theta \partial_\zeta \varphi_A) = 0. \tag{11}$$

By imposing the boundary condition that, at $\zeta = \pm\infty$, the total and relative phases are constant and that the spin is balanced so that $\cos\theta = 0$, we obtain the equation

$$\frac{\partial \varphi_B}{\partial \zeta} + \cos\theta \frac{\partial \varphi_A}{\partial \zeta} = 0 \tag{12}$$

which, after substituting into Eq. (10), yields

$$\begin{aligned} \tilde{\mathcal{L}} = &U\cos\theta \frac{\partial \varphi_A}{\partial \zeta} - \frac{1}{2} \left[\left(\frac{\partial \theta}{\partial \zeta} \right)^2 + \sin^2\theta \left(\frac{\partial \varphi_A}{\partial \zeta} \right)^2 \right] \\ &- \frac{g}{\delta g} + \frac{1}{2} \sin^2\theta + \frac{1}{3} \omega_R \sin\theta \cos\varphi_A. \end{aligned} \tag{13}$$

The variation of $\tilde{\mathcal{L}}$ with respect to φ_A and θ gives the two coupled differential equations for φ_A and θ [25]

$$\begin{aligned} &U\sin\theta \frac{\partial \theta}{\partial \zeta} + 2\sin\theta\cos\theta \frac{\partial \theta}{\partial \zeta} \frac{\partial \varphi_A}{\partial \zeta} + \sin^2\theta \frac{\partial^2 \varphi_A}{\partial \zeta^2} \\ &\qquad - \frac{\omega_R}{3} \sin\theta \sin\varphi_A = 0, \end{aligned} \tag{14}$$

$$\begin{aligned} &-U\sin\theta \frac{\partial \varphi_A}{\partial \zeta} + \frac{\partial^2 \theta}{\partial \zeta^2} - \sin\theta\cos\theta \left(\frac{\partial \varphi_A}{\partial \zeta} \right)^2 + \sin\theta\cos\theta \\ &\qquad + \frac{\omega_R}{3} \cos\theta \cos\varphi_A = 0. \end{aligned} \tag{15}$$

We point out that the same differential equations (i.e, Eqs. (12),(14),(15)) can also be derived by separating the coupled GPEs into the real and imaginary parts. Multiplying Eq. (14) by $\partial\varphi_A/\partial\zeta$ and Eq. (15) by $\partial\theta/\zeta$ and then adding them together, one can prove that the quantity

$$\begin{aligned} \tilde{\mathcal{G}} = &-\frac{1}{2} \left[\left(\frac{\partial \theta}{\partial \zeta} \right)^2 + \sin^2\theta \left(\frac{\partial \varphi_A}{\partial \zeta} \right)^2 \right] \\ &+ \frac{g}{\delta g} - \frac{1}{2} \sin^2\theta - \frac{1}{3} \omega_R \sin\theta \cos\varphi_A, \end{aligned} \tag{16}$$

is position independent, i.e, $d\tilde{\mathcal{G}}/d\zeta = 0$. The boundary conditions at $\zeta = \pm\infty$ imply $\tilde{\mathcal{G}} = (g/\delta g - 1/2 - \omega_{\rm R}/3)$. Taking into account this expression, we can rewrite Eq. (16) as

$$-\frac{1}{2}\left[\left(\frac{\partial\theta}{\partial\zeta}\right)^2 + \sin^2\theta\left(\frac{\partial\varphi_A}{\partial\zeta}\right)^2\right] + \frac{1}{2}\cos^2\theta + \frac{1}{3}\omega_{\rm R}(1-\sin\theta\cos\varphi_A) = 0. \quad (17)$$

One can understand the physical origin of the integral $\tilde{\mathcal{G}}$ by noticing that, if we consider ζ as a time variable, the quantity $\tilde{\mathcal{L}}$ in Eq. (13) is the *time-independent* Lagrangian of a mechanical system with two degrees of freedom φ_A and θ. Then it is immediately clear that $\tilde{\mathcal{G}}$ is the *conserving* energy of this auxiliary mechanical system. It is important to stress, that $\tilde{\mathcal{G}}$ is different from the actual energy density of the gas $\tilde{\mathcal{H}} = \mathcal{H}/nmc_{\rm s}^2$ which can be obtained from $\tilde{\mathcal{G}}$ by changing the sign of the first term in Eq. (16).

As will be explored below, Eq. (17) provides a very useful relation between the boundary conditions at infinity and at $\zeta = 0$. This relation will be crucial for the determination of the solutions corresponding to the magnetic solitons.

B. Energy of the magnetic solitons

For a moving magnetic soliton the analytical expression of its energy is not accessible. However the numerical solution of the above differential equations allow us to obtain the energy-velocity curve accurately, which is crucial to understand the physical properties of these solitons. As usual, the energy of a magnetic soliton can be evaluated as the difference between the canonical energies in the presence and in the absence of the soliton (see Ref. [28], Chap.5). Thus we have

$$E = \frac{n\hbar c_{\rm s}}{2}\int d\zeta\left[\left(\frac{1}{2}\left(\partial\theta/\partial\zeta\right)^2 + \frac{1}{2}\sin^2\theta\left(\partial\varphi_A/\partial\zeta\right)^2 + \frac{1}{2}\cos^2\theta + \frac{1}{3}\omega_{\rm R}(1-\sin\theta\cos\varphi_A)\right]. \quad (18)$$

The integrand of the above equation is the difference of the dimensionless energy densities $\tilde{\mathcal{H}}$, in the presence and in the absence of the soliton. The derivative terms in Eq. (18) can be eliminated using Eq. (17). Finally, we find

$$E = \frac{n\hbar c_{\rm s}}{2}\int d\zeta\left[\cos^2\theta + \frac{2}{3}\omega_{\rm R}(1-\sin\theta\cos\varphi_A)\right]. \quad (19)$$

Once we find the solutions of the magnetic solitons, i.e, θ and φ_A, the corresponding soliton energy can be readily obtained by integration. Although the velocity does not explicitly enter the above equation, the energy of the soliton still depends on it since φ_A and θ are velocity dependent. The effective mass, fixed by the velocity dependence of the energy according to the definition

$$m^* = \frac{1}{V}\frac{dE}{dV}, \quad (20)$$

can be extracted from the accurate numerical plot of the E-V curve (see Fig. (6)).

III. ANALYTICAL RESULTS

Analytic expressions for the magnetic solitons can be obtained in special cases that will be discussed in this section.

A. Static Son-Stephanov domain wall

As a first example we recover the static Son-Stephanov domain wall solution characterized by a relative phase jump of 2π in a spin-balanced system [13]. By taking $U = 0$ and $\theta = \pi/2$, the differential equation (14) for the relative phase becomes

$$\frac{\partial^2\varphi_A}{\partial\zeta^2} - \frac{\omega_{\rm R}}{3}\sin\varphi_A = 0, \quad (21)$$

which is the well-known Sine-Gordon equation whose solution is given by

$$\varphi_A = \pm 4\arctan e^{\zeta\sqrt{\omega_{\rm R}/3}} = \pm 4\arctan e^{\kappa z}, \quad (22)$$

with $\kappa = \sqrt{2m\Omega/\hbar}$ being the inverse of the characteristic width of the relative phase domain wall

$$\xi_{\rm phase} = \kappa^{-1} = \xi_{\rm s}\sqrt{\frac{3}{\omega_{\rm R}}}. \quad (23)$$

The analytic expression for the relative phase of the static domain wall (see Eq. (22)) allows us to calculate the energy of the solution explicitly. One finds:

$$E_{\rm SS} = 4n\hbar\sqrt{\frac{\hbar\Omega}{2m}} = 4n\hbar c_{\rm s}\sqrt{\frac{\omega_{\rm R}}{3}}, \quad (24)$$

and thus the dimensionless energy is $2E_{\rm SS}/n\hbar c_{\rm s} = 8\sqrt{\omega_{\rm R}/3}$.

Son and Stephanov have proven that this solution corresponds to a local minimum of the energy functional if the condition (2) is satisfied [13]. In terms of dimensionless quantities, the condition (2) can be expressed as:

$$\omega_{\rm R} < \omega_{\rm R}^{\rm c} \equiv 1. \quad (25)$$

Notice that there are two solutions for the static domain wall: one exhibiting a $+2\pi$ phase jump and the other exhibiting a -2π phase jump. Moving magnetic domain walls can be developed from either of these static domain walls and we will focus on the solutions connected to the former one.

B. Moving domain wall for weak Rabi coupling

The second example is the moving domain wall (2π magnetic soliton) whose properties can be obtained analytically in the small Rabi coupling limit

$$\omega_{\mathrm{R}} \ll 1. \tag{26}$$

Under this condition, the width of the domain wall becomes much larger than the spin healing length (see Eq. (23)):

$$\xi_{\mathrm{phase}} \gg \xi_{\mathrm{s}}, \tag{27}$$

and consequently differentiation with respect to ζ gives a small factor proportional to $\sqrt{\omega_{\mathrm{R}}}$. Eq. (15) then reduce to the simplified form:

$$\cos\theta = U\partial_\zeta \phi_A. \tag{28}$$

Integration with respect to z gives a simple analytic expression for the total magnetization

$$\int_{-\infty}^{+\infty} \cos\theta dz = 2\pi\xi_s U. \tag{29}$$

Substituting Eq. (28) into Eq. (14), after neglecting higher order terms, we obtain the differential equation for the relative phase:

$$\left(1-U^2\right)\partial_\zeta^2\varphi_A - \frac{\omega_{\mathrm{R}}}{3}\sin\varphi_A = 0. \tag{30}$$

The similarity between this equation and the Son-Stephanov differential equation (Eq. (21)) indicates that all the results holding at $U=0$ can be generalized to $U\neq 0$ by changing $\omega_{\mathrm{R}} \to \omega_{\mathrm{R}}\left(1-U^2\right)$ or $\Omega \to \Omega/\left(1-U^2\right)$. In particular the solution for the relative phase of the moving domain wall is

$$\varphi_A(U) = 4\arctan\left[\exp(\kappa(U)z)\right], \tag{31}$$

with the width of the wall

$$\xi_{\mathrm{phase}}\left(U\right) = \kappa(U)^{-1} = \xi_{\mathrm{s}}\sqrt{\frac{3(1-U^2)}{\omega_{\mathrm{R}}}}, \tag{32}$$

becoming thinner and thinner as U increases. With the help of Eq. (28) and Eq. (31), one can calculate the energy (Eq. 19) of the moving domain wall. Ignoring higher order terms in ω_{R}, one finds

$$E(U) = 4n\hbar\sqrt{\frac{\hbar\Omega}{2m(1-U^2)}} = 4n\hbar c_s\sqrt{\frac{\omega_{\mathrm{R}}}{3(1-U^2)}}, \tag{33}$$

which is actually the same expression for the energy of the static Son-Stephanov domain wall (see Eq. (24)) with ω_{R} replaced by $\omega_{\mathrm{R}}/(1-U^2)$. Furthermore, using the definition for the effective mass, we find

$$m^*(U) = \frac{1}{V}\frac{dE}{dV} = \frac{4n\hbar}{c_{\mathrm{s}}}\sqrt{\frac{\omega_{\mathrm{R}}}{3}}\frac{1}{(1-U^2)^{3/2}}. \tag{34}$$

Thus, the effective mass increases as the increase of U. However, we emphasize that the equations derived in this section are not valid when $1-U^2$ is very small. For small velocity one finds $m^*/m = 8n\xi_{\mathrm{s}}\sqrt{\omega_{\mathrm{R}}/3}$. The positiveness of the effective mass ensures the stability of the moving domain wall against snake instability. It is worth noticing that we derived the above analytical results under the assumption in Eq. (26). The positiveness of m^* at small velocity is however ensured also for finite values of ω_{R}, as long as $\omega_{\mathrm{R}} < 1$ (see below).

IV. APPLICATION OF THE THEORY: GENERAL SOLUTIONS FOR THE MAGNETIC SOLITONS

As illustrated in the introduction, after a static Son-Stephanov domain wall is imprinted in a trapped binary condensate, the domain wall starts moving and two types of solitons emerge afterwards, oscillating in the trap. In this section, we obtain the exact numerical solutions for both types of magnetic solitons in uniform matter. Both solutions must satisfy the differential equations formulated in Sec. II. However different boundary conditions should be imposed to identify the two different solutions. The difference of the boundary conditions mainly affects the behavior of the relative phase.

A. 2π solitons

The relative phase of these solitons exhibits the same 2π asymptotic phase jump as in the static case. However, the spin population becomes imbalanced in the wall center as soon as the velocity is different from zero. The boundary conditions of the 2π solitons are

$$\theta(\zeta=\pm\infty) = \frac{\pi}{2}, \varphi_A(\zeta=-\infty) = 0, \varphi_A(\zeta=+\infty) = 2\pi, \tag{35}$$

and we will look for solutions characterized by the following symmetry properties with respect to the wall center $\zeta = 0$:

$$\varphi_A(-\zeta) = 2\pi - \varphi_A(\zeta), \qquad \theta(-\zeta) = \theta(\zeta), \tag{36}$$

which implies $\varphi_A(0) = \pi$, $\partial_\zeta\theta|_{\zeta=0} = 0$. With the help of Eq. (17), a relation between the boundary conditions for φ_A and θ at $\zeta = 0$ can be established and hence one finds the slope of the relative phase as

$$\left(\frac{\partial\varphi_A}{\partial\zeta}\right)^2_{\zeta=0} = \frac{\cos^2\theta_0 + \frac{2}{3}\omega_{\mathrm{R}}(1+\sin\theta_0)}{\sin^2\theta_0}, \tag{37}$$

where the value of $\theta_0 = \theta(\zeta=0)$ determines the magnetization at the center of the soliton: $m_0 \equiv m(\zeta = 0) = \cos\theta_0$. Equation (37), a direct consequence of the boundary conditions at $\zeta = \pm\infty$, is important because it provides a boundary condition at $\zeta = 0$ which is much

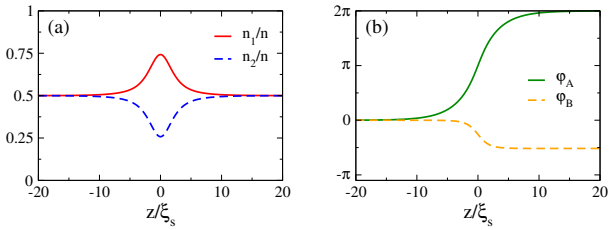

FIG. 3. Profiles of the 2π soliton with velocity $V/c_s = 0.28$, $m_0 = 0.48$, and Rabi coupling $\omega_R = 0.3$. (a) The red solid and blue dashed lines are the density distributions of the two components, satisfying $(n_1 + n_2)/n = 1$. (b) The green solid and orange dashed lines are the relative phase φ_A and total phase φ_B as a function of the coordinate. The jump of the relative phase is 2π, independent of the velocity. This solution is close to the critical velocity where the effective mass diverges (see discussion in Sec. V).

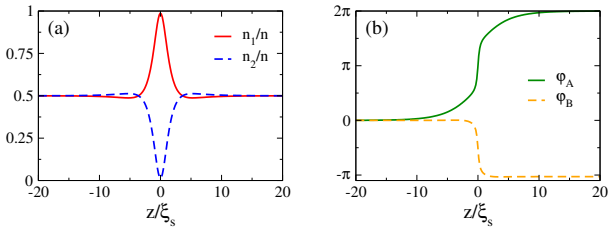

FIG. 4. Profiles of the 2π soliton with velocity $V/c_s = -0.25$, $m_0 = 0.97$ and Rabi coupling $\omega_R = 0.3$. (a) The red solid and blue dashed lines are the density distributions of the two components, satisfying $(n_1+n_2)/n = 1$. Note that two nodes appear at the wings of the soliton. (b) The green solid and orange dashed lines are the relative phase φ_A and total phase φ_B as a function of the coordinate. This soliton has a negative effective mass and corresponds to the solution very close to the green cross point with $m_0 = 1$ in Fig. 6.

more useful in order to find the solitonic solutions rather than fixing the boundary conditions at infinity.

The procedure to find the solutions of the above coupled differential equations, i.e, Eq. (14) and Eq. (15), is the following: for a given velocity U and Rabi-coupling strength ω_R, we carefully tune the input parameter θ_0 until the solution of these differential equations converge to a form satisfying the boundary conditions in Eq. (35) for the magnetic solitons [29]. The two possible signs for the slope are related to the two static Son-Stephanov domain wall solutions as $U \to 0$ and $m_0 \to 0$.

Figure 3 and Fig. 4 show the density distributions and the relative and total phases of a 2π soliton with positive ($U = V/c_s = 0.28$) and negative ($U = V/c_s = -0.25$) velocities, respectively. The difference between the two cases is that they correspond, respectively to a solution before and after the turning point (see Fig. 2). The latter case is characterized by a much higher magnetization (close to 1). For a negative velocity with even larger $|U|$ (larger evolution times in Fig. 2) the density of one component vanishes at $\zeta = 0$ and the 2π soliton breaks off, being converted into a 0π soliton.

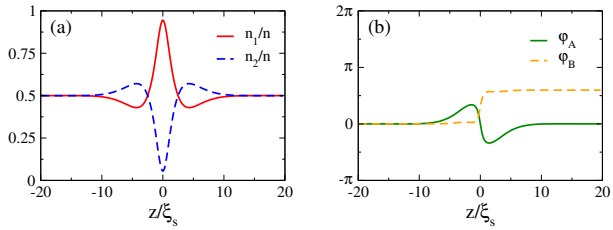

FIG. 5. Profiles of the 0π soliton with velocity $V/c_s = -0.9$, $m_0 = 0.89$ and Rabi coupling $\omega_R = 0.3$. (a) The red solid and blue dashed lines are the density distributions of the two components, satisfying $(n_1 + n_2)/n = 1$. (b) The green solid and orange dashed lines are the relative phase φ_A and total phase φ_B as a function of the coordinate. This 0π soliton has a negative effective mass and the asymptotic jump of φ_A is zero.

B. 0π solitons

Let us now discuss the main features of 0π solitons. Our results, based on GPEs simulations, show that a 2π soliton transforms into a 0π soliton when the density of one component vanishes at $\zeta = 0$ where its phase is not well-defined and thus can change by 2π without any energy cost. Although the asymptotic 2π phase jump disappears, the relative phase still varies as a function of position. The boundary conditions now become

$$\theta(\zeta = \pm\infty) = \frac{\pi}{2}\,, \quad \varphi_A(\zeta = \pm\infty) = 0, \tag{38}$$

and the natural symmetries of the φ and θ functions are

$$\varphi_A(-\zeta) = -\varphi_A(\zeta)\,, \quad \theta(-\zeta) = \theta(\zeta), \tag{39}$$

which implies $\varphi_A(0) = 0, \partial_\zeta\theta|_{\zeta=0} = 0$. Using Eq. (17), analogously to the derivation of Eq. (37), we obtain the slope of the relative phase at the soliton center as

$$\left(\frac{\partial\varphi_A}{\partial\zeta}\right)^2_{\zeta=0} = \frac{\cos^2\theta_0 + \frac{2}{3}\omega_R(1-\sin\theta_0)}{\sin^2\theta_0} \tag{40}$$

where $\theta_0 = \theta(\zeta = 0)$ determines the magnetization of the 0π soliton at $\zeta = 0$.

The procedure for finding the solutions is similar to the one developed in the previous section: for a given velocity U and Rabi-coupling strength ω_R, we can tune θ_0 until the solution of the above differential equations is consistent with the boundary conditions in Eq. (38).

Figure 5 shows the profile of a 0π soliton with negative velocity $U = V/c_s = -0.9$. The density is magnetized in the solitonic region and has two spin balanced points followed by two oppositely magnetized regions on the wings. We remind that the relative phase of the 0π soliton is an odd function of ζ and does not exhibit any asymptotic phase jump. Below we will show that, as the velocity increases, more and more oscillations will appear in the profile of 0π solitons.

V. PHASE DIAGRAM AND PROPERTIES OF MAGNETIC SOLITONS

A. Magnetization and energy

Our main results are presented in Fig. 6 where we show the curves for three different values of ω_R: $\omega_R = 0.3$, 1 and 2, which correspond to less than, equal to, and larger than the critical value (2) for the Rabi coupling below which the Son-Stephanov solution for the domain wall is stable. In both panels, the solid lines without circles label the results for the 2π solitons which exhibit a 2π relative phase jump while the solid lines with circles label 0π solitons which do not exhibit an asymptotic relative phase jump.

It is easy to recognize that the origin of Fig. 6(a), the solution with $U = 0$ and $m_0 = 0$, is the Son-Stephanov static domain wall. As shown by the red curve in Fig. 6(b), this solution is a local minimum of the E-V curve as long as $\omega_R < 1$. The effective mass of solitons (see Eq. (20)) is related to the slope of the E-V line. As shown in Fig. 6(b), the effective mass of a 2π soliton can be positive or negative when the Rabi coupling is smaller than the critical value ($\omega_R < 1$), while it is always negative when $\omega_R \geq 1$. In contrast, the effective mass of 0π soliton is always negative, irrelevant of the strength of Rabi coupling. Notice that 2π solitons with positive effective mass are not affected by snake instability.

Let us now discuss in more details the phase diagram of Fig. 6.

(i) $\omega_R < 1$. This is the most interesting case, where a 2π magnetic soliton with positive effective mass is predicted to exist. Moving continuously from the solution at the origin ($U = 0$) of Fig. 6(a), the solution exists also for finite values of U and is associated with a positive effective mass and a finite value of the magnetization (red arrow and its opposite direction). The effective mass of such solutions diverges at a critical value of the velocity (indicated with a green square in the figure). The profiles for the densities and phases at this critical point have been shown in Fig. 3. 2π solitonic solutions with larger values of $|U|$ do not exist. However 2π solitons with smaller $|U|$ and larger magnetization exist as clearly shown by Fig. 6(a), their effective mass becoming negative. Near the point (green cross in the figure) where the velocity changes sign, two nodes appear on the wings of the 2π magnetic soliton as shown in Fig. 4. The non-monotonic dependence of the magnetization on the velocity of the soliton (see Fig. 6(a)) is responsible for the loop of the energy as a function of V in the same interval of velocities (see Fig. 6(b)).

When $|m_0| = 1$, i.e. when the density of one component vanishes, the corresponding phase is not defined. Then the 2π relative phase jump disappears and a 0π solitonic solution (solid line with circles emerges at larger $|U|$. The profiles of the density and of the phases of a typical 0π solitonic solutions are shown in Fig. 5. The 0π solitonic solution continues by increasing the velocity with the corresponding decrease of magnetization until it reaches a critical velocity $U_L = V_L/c_s$ where the solitonic solution disappears, its energy approaching zero (see below).

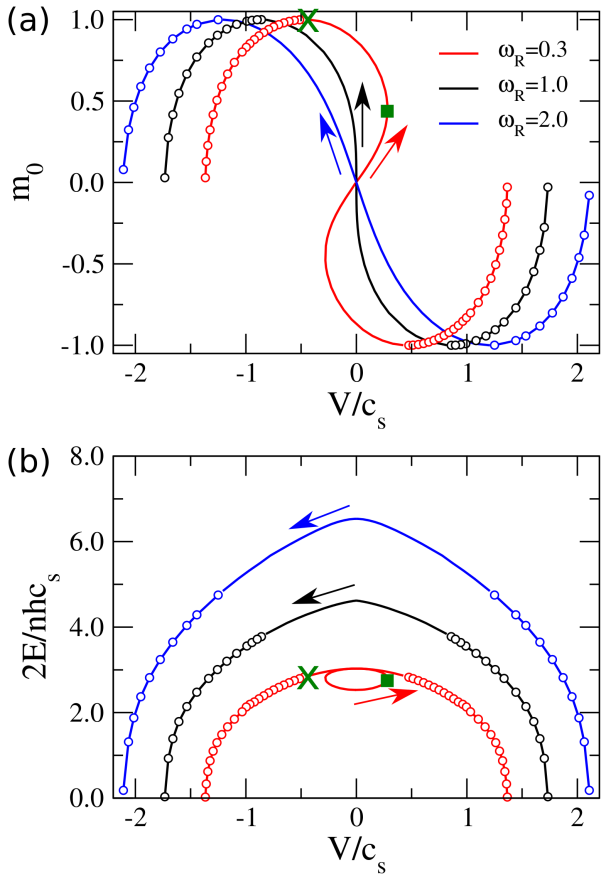

FIG. 6. (a) Phase diagram of magnetic solitons in the m_0-U plane, where m_0 is the magnetization at the center of the soliton and $U = V/c_s$ is the velocity. (b) Velocity dependence of the energy of magnetic solitons for different Rabi coupling strengths $\omega_R = 0.3$(red), 1(black) and 2(blue). The solid lines indicate that the solutions are the 2π solitons whereas the lines with circles indicate that the solutions are 0π solitons. The origin point of the upper panel corresponds to the solution of the known static Son-Stephanov domain wall with a $+2\pi$ relative phase jump and its energy increases as the Rabi coupling increases (see the lower panel). The green square indicates the solution where the effective mass of the 2π soliton diverges and the green cross indicates the position of the transformation between 2π and 0π solitons for $\omega_R = 0.3$. Note that there exists another series of solutions obtained by changing the upper panel according to the transformation $V \to -V$, then the solutions are connected to the know static Son-Stephanov domain wall with a -2π relative phase jump.

(ii) $\omega_R \geq 1$. In this case the magnetic solitons emerging from the solution of the coupled differential equations derived in Sec. II are characterized by a monotonic behavior of the magnetization as a function of the velocity (see the blue curve in Fig. 6(a)). The energy of the soliton

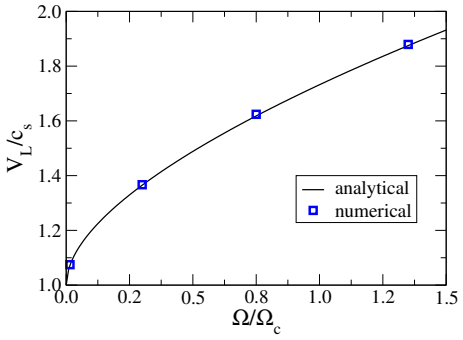

FIG. 7. Landau critical velocity for the disappearance of 0π magnetic solitons as a function of the Rabi-coupling. The solid line is the analytic prediction and the blue squares are the numerical results extracted from Fig. 6(b) (the velocity for the points where the energy of the 0π solitons tend to zero.)

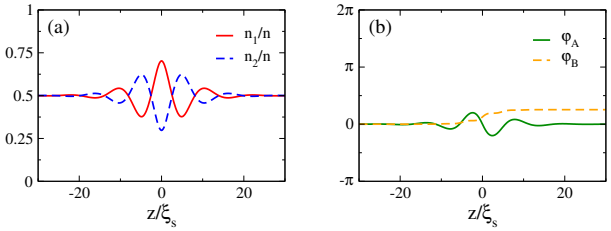

FIG. 8. Profiles of the 0π magnetic soliton with velocity $V/c_s = -1.3$, $m_0 = 0.405$ and Rabi coupling $\omega_R = 0.3$. (a) The red solid and blue dashed lines are the density distributions of the two components, satisfying $(n_1 + n_2)/n = 1$. (b) The green solid and orange dashed lines are the relative phase φ_A and total phase φ_B as a function of the coordinate. For 0π solitons the asymptotic jump of φ_A is zero. Compared to Fig. 5, there are more oscillations because the velocity of the soliton is close to the Landau critical velocity.

decreases when $|U|$ increases, corresponding to a negative effective mass(see the blue curves in Fig. 6(b)).

The case $\omega_R = 1$ (see the black curve in Fig. 6(a)), corresponding to the boundary of stability of the Son-Stephanov domain wall, is a special one. At this value of ω_R, the "polarizability" $d(m_0)/dU \to \pm\infty$ when $U \to \pm 0$. The singularity on the black curve at $U = 0$ in Fig. 6(b) is related to this divergency.

Further investigation of these solutions should concern their stability since the 2π soliton with $U = 0$, i.e, the Son-Stephanov domain wall solution, is not stable in uniform matter for $\omega_R \geq 1$ [13, 30]. The investigation of the stability conditions of magnetic solitons for $\omega_R \geq 1$ lies however beyond the scope of this work which is mainly addressed to the $\omega_R < 1$ case.

B. Landau critical velocity of 0π solitons

The phase diagram in Fig. 6 shows that 0π magnetic solitons will eventually disappear (i.e, the energy $E \to 0$) when their velocity tends to a critical value. This critical velocity (hereafter called Landau's critical velocity) is determined by the Landau's criterion

$$V_L = \min_p \frac{\varepsilon_s(p)}{p}, \tag{41}$$

associated with the emergence of an energetic instability in the dispersion of the Bogliubov spectrum

$$\varepsilon_s = \sqrt{\left(\frac{\hbar^2 k^2}{2m} + \hbar\Omega\right)\left(\frac{\hbar^2 k^2}{2m} + \hbar\Omega + n\delta g\right)} \tag{42}$$

of spin excitations in the presence of Rabi coupling [31, 32]. Using Eq. (41) one finds the result

$$\frac{V_L}{c_s} = \sqrt{1 + \frac{2\hbar\Omega}{n\delta g} + \sqrt{\frac{2\hbar\Omega}{n\delta g}\left(\frac{2\hbar\Omega}{n\delta g} + 2\right)}}$$

for the Landau's critical velocity which, in dimensionless form, reads

$$U_L = \sqrt{1 + \frac{2\omega_R}{3} + 2\sqrt{\frac{\omega_R}{3}\left(1 + \frac{\omega_R}{3}\right)}}. \tag{43}$$

Fig. 7 shows that the critical velocity extracted from the phase diagram in Fig. 6 is in excellent agreement with the above analytic prediction.

It is worth noticing that when the velocity of the 0π soliton tends to the Landau critical velocity, not only its amplitude decreases but also its structure changes. The number of oscillations in the magnetization increases and the soliton turns into a wide oscillating object in space (see Fig. 8). This fact is in accordance with the so-called theory of soliton bifurcation discussed in Ref [33].

VI. DYNAMICS IN A 1D HARMONIC TRAP

In the above sections, we focused on the exact solutions for 2π and 0π solitons propagating in uniform matter, where their shape and velocity remain unchanged during the motion. However, real experiments are always implemented in trapped systems, where the density of the condensate varies as a function of position. The amplitude and velocity of magnetic solitons are then expected to change in the trap. In this section, we discuss the dynamics of magnetic solitons in a 1D harmonic trapping potential $V(z) = m\omega_{ho}^2 z^2/2$ with ω_{ho} as the trapping frequency, using time-dependent coupled GPEs, corresponding to the Lagrangian density Eq. (3) and the energy density Eq. (4), exploiting in a more systematic way the main features anticipated in the introduction.

In Fig. 9 and Fig. 10, we track the trajectories of the magnetic solitons after the imprint of a Son-Stephanov domain wall at z_0 for a complete oscillation period. Note that the external Rabi coupling Ω is a constant for each simulation. However, in the presence of harmonic trap,

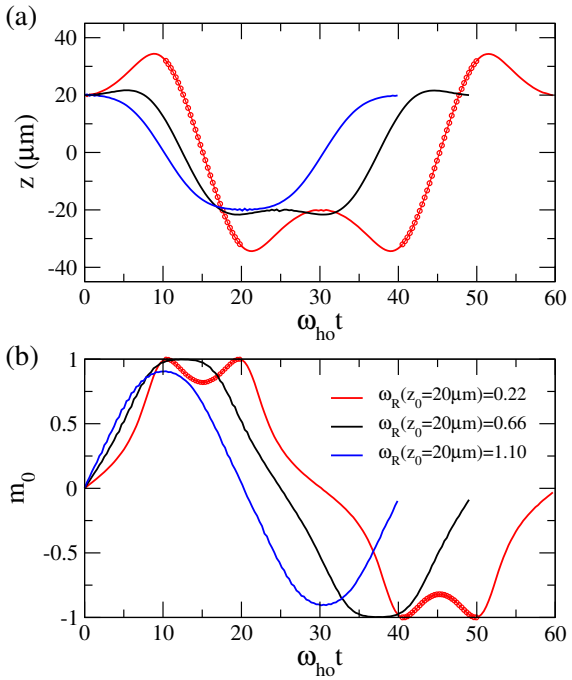

FIG. 9. (a) In-trap trajectories of magnetic solitons and (b) evolution of the magnetization m_0 at the soliton center after imprinting a Son-Stephanov domain wall at z_0 for different values of the local Rabi coupling $\omega_{\rm R}(z_0) = \Omega/\Omega_{\rm c}(z_0) = 0.22$ (red), 0.66 (black), 1.1 (blue). The solid lines indicate 2π solitons while the solid lines with circles indicate the 0π solitons. The spin-interaction parameters have been chosen the same as in ^{23}Na where $\delta g = 0.07g$ and the Thomas-Fermi radius is $R_{\rm TF} = 70\mu m$. All the curves presented here correspond to a time interval of an oscillation period.

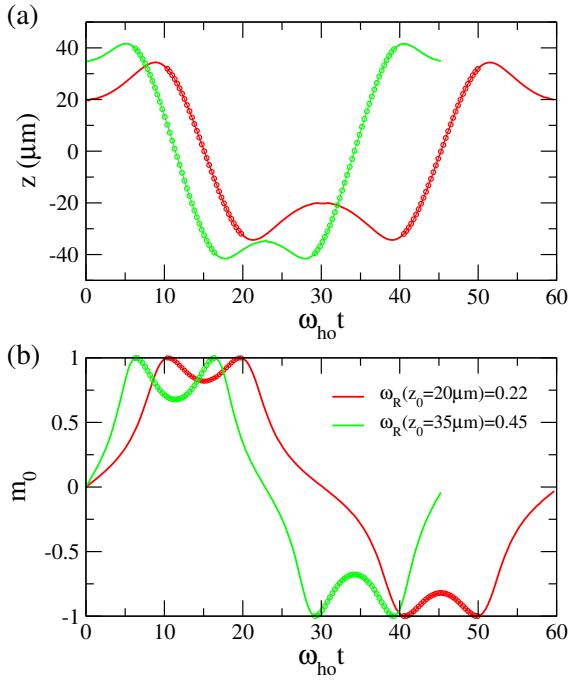

FIG. 10. (a) In-trap trajectories of the magnetic solitons and (b) the evolution of the magnetization m_0 at the soliton center after imprinting a Son-Stephanov domain wall at different initial positions $z_0 = 20\mu m$ (red) and $35\mu m$ (blue). The corresponding local dimensionless Rabi coupling are $\omega_{\rm R}(z_0) = 0.22$ (red) and 0.45 (blue), respectively. The solid lines indicate 2π solitons while the solid lines with circles indicate the 0π solitons. The spin-interaction parameters have been chosen the same as ^{23}Na with $\delta g = 0.07g$ and the Thomas-Fermi radius is $R_{\rm TF} = 70\mu m$.

the density varies and the local dimensionless Rabi coupling $\omega_{\rm R}(z) = \Omega/\Omega_{\rm c}(z)$ is also position dependent, its value being minimum at the trap center and very large near the border of the atomic cloud.

In Fig. 9, we study the oscillation dynamics of the magnetic solitons for different values of Rabi-coupling Ω (and thus different values of $\omega_{\rm R}(z_0)$) after imprinting a domain wall at the same initial position $z_0 = 20\mu m$. With the increase of $\omega_{\rm R}(z_0)$, the region exhibiting 0π solitons shrinks and eventually disappears. Furthermore, the anharmonic oscillations in the presence of both 2π and 0π magnetic solitons (see the red curve) tend to become harmonic when 0π solitons are no longer produced during the oscillation. The black curve corresponds to the case when 0π solitons no longer emerge during the oscillation. The blue curve reveals that, a 2π soliton, imprinted in a 1D harmonically trapped condensate under the condition $\omega_{\rm R}(z_0) > \omega_{\rm R}^{\rm c}(z_0)$ of the Rabi coupling, despite of its instability [13], exhibits a regular oscillation moving first towards the center of the trap because of its negative effective mass.

The analysis of Fig. 9 shows that, in order to observe the emergence of both 2π and 0π solitons during the oscillation, the local Rabi coupling at the initial position z_0 should be significantly smaller than $\omega_{\rm R}^{\rm c}(z_0)$.

In Fig. 10, we study the oscillation dynamics of the magnetic solitons for different initial positions of the phase imprinting. For larger z_0, the density of the condensate is smaller and thus $\omega_{\rm R}(z_0)$ is larger. In this case, the 2π magnetic soliton reaches the turning point faster and the 0π soliton appears earlier.

Finally, we remark that although our theory has been based on the assumption of condition (1), similar phenomena also occurs for larger values of δg where the total density exhibits a dark soliton. To demonstrate this, we will relax the condition (1) and present the simulation dynamics in the presence of larger δg in the following investigations of the role of transverse confinement.

VII. ROLE OF THE TRANSVERSE CONFINEMENT

In this section we generalize our results to two dimensional (2D) configurations, and we first consider the case of an elongated harmonic trap, with aspect ratio $\omega_\perp/\omega_{\rm ho} = 10$ where $\omega_{\rm ho}(\omega_\perp)$ is the harmonic trapping frequency along the longitudinal (transverse) direction,

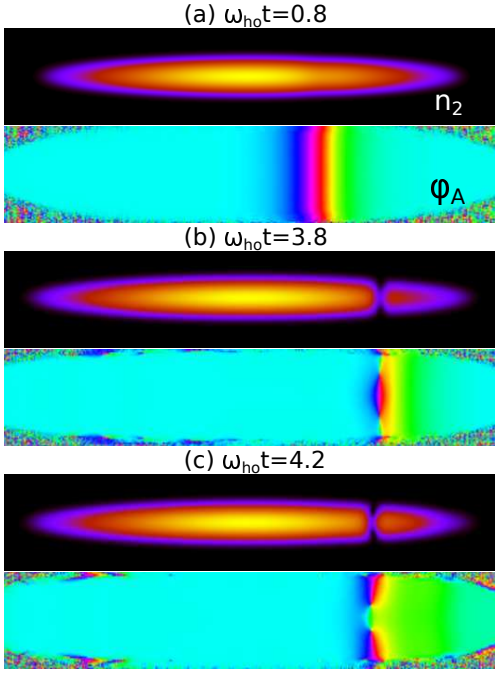

FIG. 11. Evolution of the magnetic solitons in an elongated harmonic trap (aspect ratio = 10) after imprinting a Son-Stephanov domain wall. For each time instant we show the density of the second component n_2 in the upper panel and the relative phase φ_A in the lower panel.

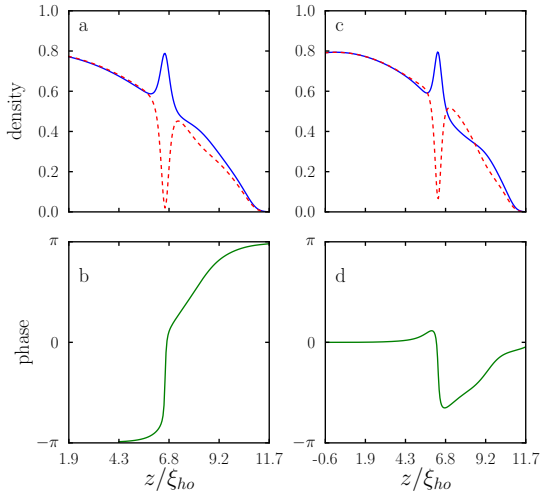

FIG. 12. Densities of the two spin components and their relative phase φ_A calculated on a cut along the longer axis of the configurations presented in Fig. 11. The figures on the left and on the right panel correspond, respectively to the soliton before ($\omega_{\rm ho}t = 3.8$) and after ($\omega_{\rm ho}t = 4.2$) reflection. We can see that the configuration before the reflection corresponds to a 2π soliton and the configuration after the reflection corresponds to a 0π soliton.

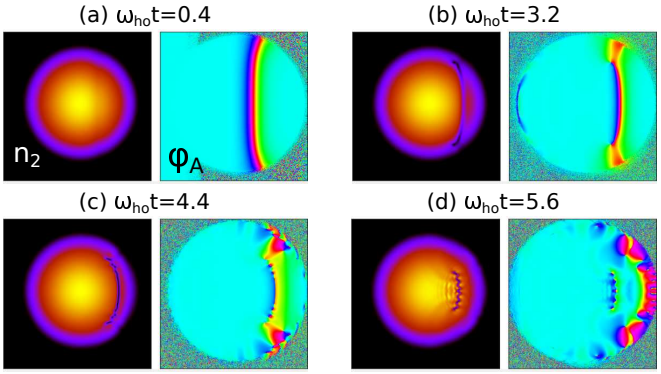

FIG. 13. Evolution of an imprinted Son-Stephanov domain wall in a spherical harmonic trap. For each time instant we show the density of the second component n_2 and the relative phase φ_A.

in order to understand how the 1D solutions behave in this elongated geometry. We expect that this elongated geometry will share many 1D features. Indeed, the domain wall characterized by a 2π relative phase jump, which was initially imprinted along the weak axis of the trap and displaced from the center by a small fraction of the Thomas-Fermi radius, begins to travel along the weak axis towards the closer edge of the cigar could. When the 2π soliton moves to the turning point, it develops a density polarization and induces two vortices at its ends, see Fig. 11. Then, it moves back towards the center of the trap as was predicted for the 1D solution, but now we observe that the domain wall is fragmented in two pieces and no longer extends through the whole transverse direction. see Fig. 11(c). As discussed in [34, 35] the end of a finite domain wall is always associated with the existence of a vortex in one of the two spin components, ensuring the proper behavior of the phase around the end point. In the region between the vortices we have a polarized density suggesting, that our solution matches the 0π magnetic soliton obtained in the 1D configuration. In Fig. 12 we show the cut of the density and phase of the gas along the weak confinement axis before and after the reflection. We can recognize the same structure as in Fig. 3 and Fig. 5 for 2π and 0π solitons, respectively.

For fully 2D configurations, the 1D dynamics of magnetic solitons discussed in the previous sections no longer applies, and the domain wall cannot oscillate indefinitely. To demonstrate this, we have repeated the numerical simulation for an isotropic harmonic potential, where the 2D physics should be fully manifested. We have assumed $\Omega = 0.5\omega_{\rm ho}$ and $\delta g = 0.4g$. Initially the domain wall travels to the edge of the trap, similar as the case of an elongated trap. However, in the presence of transverse confinement, the domain wall starts to bend and the vortices generated near the end of the wall become detached from the cloud boundary. Furthermore, the reflection is associated with a production of multiple vortices along what was formerly a single domain wall, see Fig. 13. These vortices travel back towards the center together, but soon the dynamics becomes very complicated. The excess energy is converted into phononic excitations,

and the domain wall is lost.

VIII. DISCUSSION

We have investigated the main features of moving magnetic solitons in Rabi-coupled binary Bose-Einstein condensates. Two types of magnetic solitons have been identified and characterized: (i) 2π solitons, which are connected to the unmagnetized static Son-Stephanov domain wall and exhibit a 2π relative phase jump; (ii) 0π soliton, which are connected to 2π solitons at a critical velocity, where the density of one component vanishes, and which do not exhibit a net jump of the relative phase. The complete phase diagram, the energy and the magnetic properties of these solitons are obtained in uniform matter, and their dynamical evolution is calculated in a 1D and 2D harmonic trap. A peculiar feature emerging from our calculations is that 2π solitons evolve into 0π solitons (and vice versa) during their oscillatory motion in a harmonic trap.

We expect these novel examples of solitons can be observed experimentally in the near future. To observe them in ultracold atoms one can, for example, use a mixture of the $|F = 1, m_F = +1\rangle$ and $|F = 1, m_F = -1\rangle$ hyperfine components of the $3^2S_{1/2}$ states of sodium, where $\delta g/g \approx 0.07$ [36]. For typical experimental parameters, the chemical potential is $\mu \sim h \times 10^4$Hz, and thus the critical Rabi coupling is estimated as $\Omega_c = n\delta g/3 = 0.023ng = 0.023\mu = h \times 230$Hz. Therefore, a weak Rabi coupling (the order of $\sim$ 100Hz) is required to observe these magnetic solitons, a condition easily available with current experimental techniques.

Although our discussion of magnetic solitons has been focused in the context of the binary Bose-Einstein condensates, similar physics can be easily generalized to and investigated in other physical systems which are governed by coupled GPEs, such as fiber optics [37], exciton-polaritons [38], etc.

ACKNOWLEDGMENTS

We would like to thank Gabriele Ferrari and William D. Phillips for useful discussions. This work was supported by the QUIC grant of the Horizon2020 FET program and by Provincia Autonoma di Trento. M.T is partially supported by the PL-Grid infrastructure.

[1] T. W. B. Kibble, *Topology of cosmic domains and strings*, J. Phys. A: Math. Gen., **9**, 1387 (1976).
[2] S. Emori, U. Bauer, S.-M. Ahn, E. Martinez and G. S. D. Beach, *Current-driven dynamics of chiral ferromagnetic domain walls*, Nature Materials, **12**, 611 (2013).
[3] W. P. Su, J. R. Schrieffer, and A. J. Heeger, *Solitons in Polyacetylene*, Phys. Rev. Lett. **42**, 1698 (1979).
[4] L. F. Mollenauer, R. H. Stolen, and J. P. Gordon, *Experimental Observation of Picosecond Pulse Narrowing and Solitons in Optical Fibers*, Phys. Rev. Lett. **45**, 1095 (1980).
[5] G. Lamporesi, S. Donadello, S. Serafini, F. Dolfovo, and G. Ferrari, *Spontaneous creation of KibbleZurek solitons in a BoseEinstein condensate*, Nature Physics **9**, 656 (2013).
[6] S. Burger, K. Bongs, S. Dettmer, W. Ertmer, K. Sengstock, A. Sanpera, G. V. Shlyapnikov, and M. Lewenstein, *Dark Solitons in Bose-Einstein Condensates*, Phys. Rev. Lett. **83**, 5198 (1999).
[7] J. Denschlag *et al.*, *Generating Solitons by Phase Engineering of a Bose-Einstein Condensate*, Science **287**, 97 (2000).
[8] L. Khaykovich, F. Schreck, G. Ferrari, T. Bourdel, J. Cubizolles, L. D. Carr, Y. Castin, C. Salomon, *Formation of a Matter-Wave Bright Soliton*, Science **296**, 1290 (2002).
[9] Th. Busch and J. R. Anglin, *Dark-Bright Solitons in Inhomogeneous Bose-Einstein Condensates*, Phys. Rev. Lett. **87**, 010401 (2001).
[10] C. Becker, S. Stellmer, P. Soltan-Panahi,S. Dörscher, M. Baumert, E.M. Richter, J. Kronjäger, K. Bongs, and K. Sengstock, *Oscillations and interactions of dark and darkbright solitons in BoseEinstein condensates*, Nature Physics **4**, 496 (2008).
[11] X. Liu, H. Pu, B. Xiong, W. M. Liu and J. Gong, *Formation and transformation of vector solitons in two-species Bose-Einstein condensates with a tunable interaction*, Phys. Rev. A **79**, 013423 (2009).
[12] C. Hamner, J. J. Chang, P. Engels, and M. A. Hoefer, *Generation of Dark-Bright Soliton Trains in Superfluid-Superfluid Counterflow*, Phys. Rev. Lett. **106**, 065302 (2011).
[13] D. T. Son and M. A. Stephanov, *Domain walls of relative phase in two-component Bose-Einstein condensates*, Phys. Rev. A **65**,063621 (2002).
[14] M. R. Matthews, B. P. Anderson, P. C. Haljan, D. S. Hall, C. E. Wieman, and E. A. Cornell, *Vortices in a Bose-Einstein Condensate*, Phys. Rev. Lett. **83**, 2498 (1999).
[15] M. W. Zwierlein, J. R. Abo-Shaeer, A. Schirotzek, C. H. Schunck and W. Ketterle, *Vortices and superfluidity in a strongly interacting Fermi gas*, Nature **435**, 1047 (2005).
[16] U. A. Khawaja and H. Stoof, *Skyrmions in a ferromagnetic BoseEinstein condensate*, Nature **411**, 918 (2001).
[17] L. S. Leslie, A. Hansen, K. C. Wright, B. M. Deutsch, and N. P. Bigelow, *Creation and Detection of Skyrmions in a Bose-Einstein Condensate*, Phys. Rev. Lett. **103**, 250401 (2009).
[18] M. R. Matthews, B. P. Anderson, P. C. Haljan, D. S. Hall, M. J. Holland, J. E. Williams, C. E. Wieman, and E. A. Cornell, *Watching a Superfluid Untwist Itself: Recurrence of Rabi Oscillations in a Bose-Einstein Condensate*, Phys. Rev. Lett. **83**, 3358 (1999).
[19] T. Zibold, E. Nicklas, C. Gross, and M. K. Oberthaler, *Classical Bifurcation at the Transition from Rabi to Josephson Dynamics*, Phys. Rev. Lett. **105**, 204101 (2010).
[20] C. Hamner, Y. Zhang, J.J. Chang, C. Zhang, and P.

Engels, *Phase Winding a Two-Component Bose-Einstein Condensate in an Elongated Trap: Experimental Observation of Moving Magnetic Orders and Dark-Bright Solitons*, Phys. Rev. Lett. **111**, 264101 (2013).

[21] T. Congy, A. M. Kamchatnov, and N. Pavloff, *Nonlinear waves in coherently coupled Bose-Einstein condensates*, Phys. Rev. A **93**, 043613 (2016).

[22] Note that in the presence of Rabi coupling, the stability of the mixture can be even ensured for values of $\delta g < 0$, provided the condition $\hbar\Omega > -n\delta g$ is satisfied.

[23] C. Qu, L. P. Pitaevskii, S. Stringari, *Magnetic solitons in a Binary Bose-Einstein Condensate*, Phys. Rev. Lett. **116**, 160402 (2016).

[24] T. Congy, A. M. Kamchatnov, N. Pavloff, *Dispersive hydrodynamics of nonlinear polarization waves in two-component Bose-Einstein condensates*, arXiv:1607.08760

[25] Generally speaking, the variation should be performed before substituting $\partial_\zeta \varphi_B$ into $\tilde{\mathcal{L}}$. However, in our case it is possible to first implement this substitution due to the solitonic boundary conditions imposed on φ_B. Indeed, the variation should be performed at constant φ_B. The substitution introduces additional dependence on φ_A and θ. However, this dependence does not contribute to variations, because due to Eq. (11) and Eq. (12) we get $\partial\tilde{L}/\partial\left(\partial_\zeta\varphi_B\right) = 0$. In more general cases one should performe variation of so-called Rauth function instead of function $\tilde{\mathcal{L}}$. (See, for example, Ref [26], Sec. 41 or Ref [27], Sec. 8.3.)

[26] L. D. Landau and E. M. Lifshitz, *Mechanics*, 3rd ed., (Pergamon Press, 1969)

[27] H. Goldstein, C. P. Poole Jr. and J. L. Safko, *Classical Mechanics*, 3rd ed., (Pearson Education Limited 2014).

[28] L. P. Pitaevskii and S. Stringari, *Bose-Einstein Condensation and Superfluidity*, (Oxford University Press, New York, 2016).

[29] It is worth to note that to obtain a correct solution, the parameter θ_0 should be tuned with a very high precision.

[30] A. Usui and H. Takeuchi, *Rabi-coupled countersuperflow in binary Bose-Einstein condensates*, Phys. Rev. A **91**, 063635 (2015).

[31] E. V. Goldstein and P. Meystre, *Quasiparticle instabilities in multicomponent atomic condensates*, Phys. Rev. A **55**, 2935 (1997).

[32] M. Abad and A. Recati, *A study of coherently coupled two-component Bose-Einstein condensates*, Eur. Phys. J. D **67**, 148 (2013).

[33] E. A. Kuznetsov and F. Dias, *Bifurcations of solitons and their stability*, Physics Reports **507,** 43 (2011) .

[34] M. Tylutki, L. P. Pitaevskii, A. Recati, S. Stringari, *Confinement and precession of vortex pairs in coherently coupled Bose-Einstein condensates*, Phys. Rev. A **93**, 043623 (2016).

[35] L. Calderaro, A. L. Fetter, P. Massignan, P. Wittek, *Vortex dynamics in coherently coupled Bose-Einstein condensates*, arXiv:1609.03966

[36] T. Bienaimé, E. Fava, G. Colzi, C. Mordini, S. Serafini, C. Qu, S. Stringari, G. Lamporesi, and G. Ferrari, *Spin-Dipole Oscillation and Polarizability of a Binary Bose-Einstein Condensate near the Miscible-Immiscible Phase Transition*, arXiv:1607.04574

[37] N. Akhmediev and A. Ankiewicz, *Novel soliton states and bifurcation phenomena in nonlinear fiber couplers*, Phys. Rev. Lett. **70**, 2395 (1993).

[38] D. D. Solnyshkov, H. Flayac, and G. Malpuech, *Stable magnetic monopoles in spinor polariton condensates*, Phys. Rev. B **85**, 073105 (2012).